JOURNAL OF GEOPHYSICAL RESEARCH, VOL. 98, NO. E3, PAGES 5499–5504, MARCH 25, 1993

Excitation of Positive Ions by Low-Energy Electrons: Relevance to the Io Torus

STEVEN J. SMITH,[1] A. CHUTJIAN,[1] R. J. MAWHORTER,[2]
I. D. WILLIAMS,[3] AND D. E. SHEMANSKY[4]

The importance of measuring electron-ion excitation cross sections in singly and multiply charged positive ions is outlined, and recent results for Mg II and O II ions are given using the Jet Propulsion Laboratory's electron energy-loss merged-beams apparatus. For Mg II, collision strengths are presented for the $3s\ ^2S \rightarrow 3p\ ^2P(h, k)$ resonance transition at electron energies from threshold to approximately 9 × threshold (40 eV). Theoretical comparisons are also given with two five-state close-coupling calculations. The energy variation of the collision strength is fitted with a semiempirical analytic function which includes approximations to polarization, resonance, and exchange contributions. In O II, first spectra anywhere of electron excitation of the optically allowed $2s^22p^3\ ^4S^o \rightarrow 2s2p^4\ ^4P$ (14.88 eV) and $\rightarrow 2p^23s\ ^4P$ (22.98 eV) transitions are presented. In addition, excitations of the two low lying, optically forbidden transitions $^4S^o \rightarrow 2p^3\ ^2D^o$ (3.33 eV) and $\rightarrow 2p^3\ ^2P^o$ (5.02 eV) are detected for the first time.

1. INTRODUCTION

The collisional excitation of singly and multiply charged positive ions by electrons occurs in a wide range of astronomical plasmas. Dipole-allowed and dipole-forbidden transitions in stellar and interstellar objects have long been observed by ground-based and orbiting telescopes, and most recently by the Hubble space telescope (HST) [e.g., *Carpenter et al.*, 1991]. A wide variety of ionic emission spectra is seen, including the ubiquitous (h, k) resonance transitions in Mg II, with low-energy electrons as the principal excitation means. Recently reported observations using the Hopkins ultraviolet telescope aboard the Astro 1 mission in December 1990 have revealed Mg II emission lines in supernova remnants [*Blair et al.*, 1991] and, closer to home, O II lines in the Io torus [*Moos et al.*, 1991].

Central to the understanding of energy balance in the Io torus is the rate of radiative decay via allowed and forbidden lines in neutral and ionized oxygen and sulfur [*Ballester et al.*, 1987; *Brown*, 1976, 1978; *Trauger*, 1984; *Strobel and Davis*, 1980; *Shemansky*, 1987]. Charge states of up to O IV and S V have been included in collisional models of the torus [*Shemansky and Smith*, 1981]. These were some of the species detected in the Voyager EUV measurements at Jupiter [*Broadfoot et al.*, 1981].

There are no experimental measurements of collision strengths or excitation cross sections in the ions O II–O IV or S II–S V. Modeling calculations of the torus have had to rely on theoretical oscillator strengths and collision strengths [*Ho and Henry*, 1983*a*, *b*, 1984; *Aggarwal and Hibbert*, 1991; *Bell et al.*, 1991]. These calculations are quite extensive, involving good configuration-interaction wavefunctions with a many-channel, close-coupling scattering approximation. Nevertheless, it would be valuable to have experimental verification of the calculated collision strengths. Resonances exist at threshold which can enhance cross sections for optically allowed transitions by factors of 2, and by even larger factors for optically forbidden transitions. Experimental measurements would reveal these resonances and provide an independent check as to whether they were being described adequately by theory.

We describe in section 2 a new experimental method capable of measuring absolute cross sections in singly and multiply charged ions. The method is based on the electron energy-loss approach [*Chutjian and Newell*, 1982] using merged beams [*Smith et al.*, 1991]. Results are then presented in section 3 for excitation of two astronomically important ions: Mg II and O II. These results illustrate the following capabilities of the energy-loss technique: (1) measurement in the threshold region where resonances are important, and where electron-energy distribution functions have a maximum, (2) measurements above threshold, (3) measurements for optically forbidden transitions, and (4) measurements which are free of cascade effects from higher excited levels.

2. EXPERIMENTAL METHODS

A schematic diagram of the apparatus is shown in Figure 1. Singly ionized magnesium ions are generated in a discharge ion source without use of a carrier gas. Singly ionized oxygen ions are generated using CO as the feed gas. Ions are extracted through a 0.15-mm (Mg II) or 0.25-mm (O II) diameter anode hole by a three-element lens L1, and momentum analyzed in a 60° deflection magnet (DM). Ions of the appropriate mass/charge are focused by lenses L2–L4 into the center of the merged region, and thence by L5 into a deep Faraday cup. Deflector plates D are used to bend the ion beam off axis to prevent either fast, charge-exchanged neutrals, or secondary electrons in the deflection magnet from reaching the merged region.

The ion-source and deflection-magnet region are pumped by two oil diffusion pumps and one ion pump. A pumping baffle (tube) B separates the relatively low-vacuum region

[1]Jet Propulsion Laboratory, California Institute of Technology, Pasadena.
[2]Department of Physics and Astronomy, Pomona College, Claremont, California.
[3]Department of Pure and Applied Physics, The Queen's University, Belfast, United Kingdom.
[4]Department of Aerospace Engineering, University of Southern California, Los Angeles.

Paper number 92JE02807.
0148-0227/93/92JE-02807$05.00

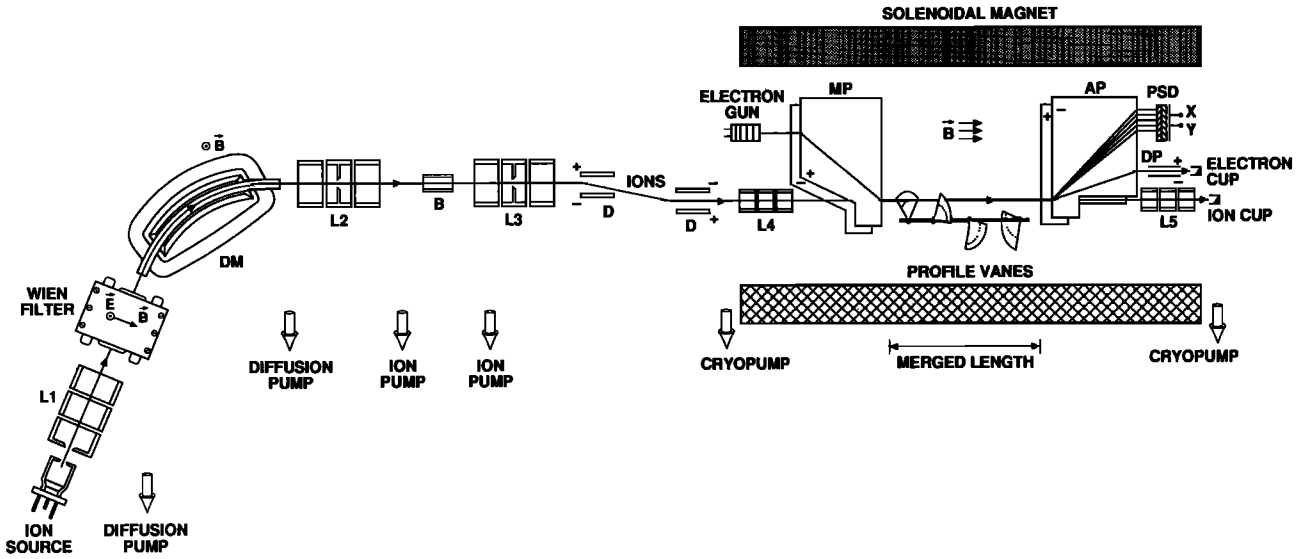

Fig. 1. Experimental setup: L1–L5, three-element focusing lenses; DM, 60° deflection magnet; B, differential pumping baffle; D, deflector plates; MP, merging trochoidal plates; AP, electron analyzing plates; DP, trochoidal deflection plates to deflect parent electron beam out of the scattering plane; and PSD, position-sensitive detector.

from the ultrahigh vacuum region. The latter is pumped by one ion pump and two cryopumps. Base pressure in the ion source region is 7×10^{-5} Pa, while that of the merged region is 1×10^{-7} Pa. Pressure in the merged region during operation of both beams is 5×10^{-7} Pa.

The low-energy electrons are merged with the ion beam in a uniform, stable solenoidal magnetic field through the use of trochoidal ($\mathbf{E} \times \mathbf{B}$ fields) deflection plates (MP) [*Auerbach et al.*, 1977; *Wåhlin et al.*, 1991]. Inelastically scattered electrons from the merged, interaction region are demerged by a second set of analyzing trochoidal plates (AP), which disperse the electrons according to their final longitudinal and radial velocities. In order to reduce background contributions from the intense parent electron beam, that beam is trochoidally deflected out of the scattering plane (defined by the directions of the incident and scattered electrons) by plates DP, and trapped in a deep Faraday cup. The density profiles in both beams are measured simultaneously using four separate vanes with radially spaced holes which take "slices" through the beams. The entire experiment is mounted on a 15-mm-thick titanium plate whose faces have been ground flat and parallel to 0.1 mm. The plate can be removed from the magnet bore along titanium rods mounted within the bore.

The inelastically scattered electrons are measured using a position-sensitive detector (PSD). The PSD is a 40-mm-diameter microchannel-plate array with a resistive anode. The front face is oriented normal to the direction of **B**, and masked by titanium plate to a viewing area of 12.7 mm high $\times$ 40.6 mm long. Three sets of 92% transmitting grids are used to carry out retarding-potential measurements on the scattered electrons. The entire unit is housed in a titanium can for shielding purposes.

Apparatus control is through a CAMAC crate. The four separate corner signal leads from the resistive anode exit the vacuum chamber, and enter a four-channel preamplifier whose output is sent to a position computer. The x, y position of each valid electron event is stored in a histogramming memory. The time spent in each beams modulation cycle is clocked through a 10-MHz clock and quad scaler. These times are stored in the PC and later used to convert signal counts into signal rates. A typical experimental run consists of about 500–1500 s of data accumulation. Each run is preceded or followed by a measurement of the beam profiles to establish the overlap integral. These profiles are measured with a microstep motor controlled by a countdown timer portion of a scaler/timer in the CAMAC crate. The scaler/timer commands the PC to drive the microstep motor (with pulses from the PC's communication port). Separate charge-pump digitizers convert the analog electron and ion currents (from the respective Faraday cups) into digital pulses, which the scaler/timer also counts. After a preset counting signal, a start command is sent to the PC, along with the stored digitized currents transmitted through the beam profile vanes. Each command to advance to a new vane position is followed by a 0.2-s "pause," which gives both beams an opportunity to "settle." This is followed by a 1- to 5-s counting period (depending upon the beam currents). These counts are then transferred to the PC, and a new vane position commanded. Profiles are measured at four locations along the 20-cm merged length, and complete profile measurement takes about 10–12 min.

The energy-loss approach. In this technique, one detects directly, in an electron-ion collision, the inelastically scattered electron [*Chutjian and Newell*, 1982]. For an ion A^{m+} of charge m^+ and initial state nl, to final state $n'l'$, the process is given by

$$e(E_e, 0°) + A^{m+}(nl, E_i) \rightarrow A^{m+}(n'l', E_i - \Delta E_i) + e(E_e - \Delta E_e, \theta) \quad (1)$$

Here, the incident electron e and ion A^{m+} have laboratory energies E_e and E_i, respectively. The inelastically scattered electron has energy $E_e - \Delta E_e$ and laboratory scattering angle θ relative to the incident electron beam ($\theta = 0°$). From conservation of energy and momentum, the inelastic energy loss ΔE_{CM} (expressed in the center-of-mass (CM) frame) absorbed during the collision (e.g., $\Delta E_{CM} = 4.43$ eV for the

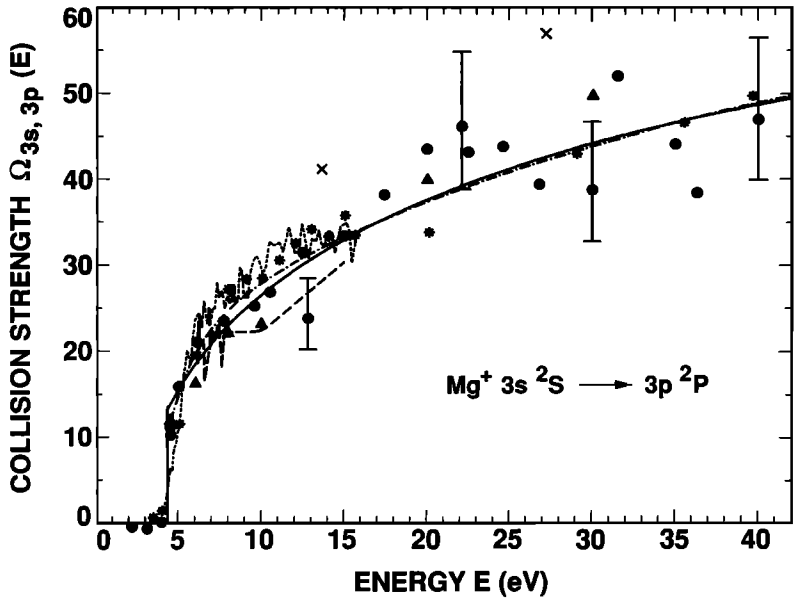

Fig. 2. Experimental and theoretical excitation cross sections for the $^2S \rightarrow {}^2P(h, k)$ transitions in Mg II. Symbols are as follows: solid circles, present measurements; stars, photon-emission measurements of *Zapesochnyĭ et al.* [1976]; dotted line, photon-emission measurements of *Zapesochnyĭ et al.* [1984]; crosses, distorted-wave, polarized-orbital calculations of *Kennedy et al.* [1978]; dashed line, 5CC(HF) in *Smith et al.* [1993]; and solid triangle, 5CC(CI) calculations in *Smith et al.* [1993]. Present analytic comparisons (from (4)) are best-fit to data (solid line) and fit constrained to $f_{3s,3p} = 0.940$ (dash-dot line).

$3s \rightarrow 3p$ transition in Mg II) is carried away by both the electron (ΔE_e) and the ion (ΔE_i) [*Brouillard and Claeys*, 1983]. The detected particle is the electron $e(E_e - \Delta E_e, \theta)$. By virtue of its spin and charge, the electron is able to excite both optically allowed and optically forbidden (so-called intersystem or forbidden) transitions in $A^{m+}(nl)$.

The merged electron and ion beam techniques. The use of merged beams, rather than crossed beams as was used in earlier work, was dictated by the need to (1) have a greater collision volume, so that signal rates would be higher, and (2) to realize an important kinematic advantage that would allow one to carry out measurements at threshold in the CM frame, but yet detect electrons having energies of ~0.2 in the laboratory frame. The excitation cross sections $\sigma_{ij}(E)$ between lower state i and upper state j, and at the CM energy E, is related to the experimental parameters by

$$\sigma_{ij}(E) = \frac{Re^2F}{\varepsilon I_i I_e L}\left|\frac{v_e v_i}{v_e - v_i}\right| \tag{2}$$

where R is the total signal rate (s^{-1}) for full $\{0, \pi\}$ angular collection in the CM frame, e the electron charge, I_e and I_i the electron and ion currents (in amperes), respectively, L the effective merged pathlength (in centimeters), v_e and v_i the electron and ion velocities (cm/s), respectively, ε the detection efficiency of the PSD, and F the overlap factor between the electron and ion beams (cm^2). Only the magnitude of the relative velocity is relevant to the scattering, so that the same CM energy can be obtained with different combinations of electron and ion velocities. This serves as a useful diagnostic of the final cross section, since the final cross section must be independent of the chosen combination.

Electron and ion beam currents are kept low so that (1) single-collision conditions apply, (2) "intermodulation effects" (the space charge of one beam altering trajectories of the other) are absent, and (3) electron and ion background rates are low, and PSD dead-time corrections kept small. There are further effects which have to be considered before deriving an absolute cross section from (2). These effects, discussed in detail in *Smith et al.* [1993] are electron spiraling, laboratory-CM energy and angle conversions, beam shear in the trochoidal deflection plates, beam profile measurement, double-beam modulation, detector calibration, overlap between elastically scattered (Coulomb) and inelastically scattered electrons on the final image on the PSD, and correction for the loss of backward-scattered electrons at energies near threshold.

3. Results in *e*-Mg II and *e*-O II Scattering

The e-Mg II Scattering

The measured excitation cross section $\sigma_{ij}(X)$ (in (2), when reported in atomic units of πa_0^2) is related to the collision strength $\Omega_{ij}(X)$ by

$$\sigma_{ij}(X) = \frac{\Omega_{ij}(X)}{\omega_i}[E_{ij}(X)]^{-1}, \tag{3}$$

where E_{ij} is the transition energy ΔE_{CM} in Rydbergs, X is the CM energy in threshold units, and $\omega_i = (2S_i + 1)(2L_i + 1)$ for LS coupling. Present measurements of collision strengths $\Omega_{3s,3p}(E)$ for the $3s\ ^2S \rightarrow 3p\ ^2P(h, k)$ transition in Mg II were combined with several theoretical five-state close-coupling (5CC) calculations [*Smith et al.*, 1993; *Mitroy and Norcross*, 1989; *Mitroy et al.*, 1988]. Results are shown in Figure 2. Experimental uncertainties are indicated at the 90% or 1.7σ confidence level. Also shown in Figure 2 are comparisons of the present data (without cascade) with optical-emission data of *Zapesochnyĭ et al.* [1976, 1984]

(with cascade); and with four sets of theoretical or semiempirical calculations: a distorted-wave calculation of *Kennedy et al.* [1978], a 5CC calculation with Hartree-Fock (HF) wave functions [*Smith et al.*, 1993], and a 5CC calculation with configuration-interaction (CI) wave functions [*Smith et al.*, 1993].

Resonance structure is predicted in the calculations. It is also predicted and noted in *Zapesochnyĭ et al.* [1984] and was, in fact, first calculated by *Burke and Moores* [1968]. Agreement of the present data with results of *Zapesochnyĭ et al.* [1976, 1984] near threshold, where cascading is absent, is within combined experimental errors. One might have expected photon-emission data lying above the $4s\ ^2S$ energy (8.66 eV) to have a cascade contribution and hence to lie above the present data. For Mg II this cascading appears to be a small effect, but a better assessment must await an accurate cascade calculation.

One finds good agreement of the present data with the distorted-wave theory and with the present 5CC(HF) and 5CC(CI) theories. The Gaunt-factor results [*Mewe*, 1972; *van Regemorter*, 1962] give cross sections which differ by factors of 2–3 (see comparisons in *Smith et al.* [1993]). This clearly speaks against the use of these approximations in astrophysical calculations, where such errors in collision strengths can lead to orders-of-magnitude error in calculation of plasma electron temperatures and densities.

The shape of the experimental excitation cross section can provide diagnostic information on the details of the electron-ion reaction, given sufficient data quality. The H_2 Lyman and Werner bands, for example, have been used, through analysis of the shape functions, to establish the contribution of the Born electric dipole component to the total cross section [*Shemansky et al.*, 1985*a*]. This was accomplished by fitting the shape function with a semiempirical analytic function designed to include approximations to polarization, resonance, and exchange components in the total cross section. The measured collision strengths reported here are fitted with an analytic function used extensively in plasma radiative-equilibrium calculations [*Shemansky*, 1988]. The code is broadly applicable in obtaining accurate fits to a wide range of excitation functions. The collision strength is given by the following functional form:

$$\Omega_{ij}(X) = C_0(X^{-2}) + \sum_{k=1}^{4} C_k \exp(-kC_8X) + C_5 + \frac{C_6}{X} + C_7 \ln(X), \quad (4)$$

where the C_k are constants of the function [*Shemansky et al.*, 1985*a*, *b*].

Thermally averaged values and rate coefficients can be obtained from [*Shemansky et al.*, 1985*a*]

$$\Omega_{ij}(T_e) = \left[C_0E_2(Y) + \left(C_6 + \frac{C_7}{Y}\right)E_1(Y)\right]Y \exp(Y) + C_5 + \sum_{k=1}^{4} C_k \frac{Y}{Y + kC_8} \exp(-kC_8), \quad (5)$$

where $Y = E_{ij}/T_e$, T_e is electron temperature in Rydbergs, and $E_n(Y)$ is the exponential integral of order n. The rate coefficient $Q_{ij}(T_e)$ ($cm^3\ s^{-1}$) is given by

$$Q_{ij}(T_e) = (2.173 \times 10^{-8})\left(\frac{Y}{E_{ij}}\right)^{1/2}\left(\frac{\Omega_{ij}(T_e)}{\omega_i}\right) \exp(-Y) \quad (6)$$

The constant C_7 in the Born term is related to the electric dipole oscillator strength by the equation

$$C_7 = \omega_i(4.00)\frac{f_{ij}}{E_{ij}}. \quad (7)$$

The Mg II data have been fitted using (4), and the result is basically compatible with the known oscillator strength for the transition. Figure 2 shows two model comparisons to the data. The first is one in which the parameters are unconstrained in obtaining a best fit to the data. The second is one in which the constant C_7 is fixed by the known oscillator strength through (7). Both give satisfactory fits to the data, although the second case produces collision strength constants that are physically unrealistic, with large cancellation between terms. The data in this case do not strongly limit the range of possible values of the oscillator strength: the highest energy herein (40 eV) is still rather low for good definition of the Born term, and the experimental uncertainty is relatively large. However, within this uncertainty there is consistency with the known value of $f_{ij} = 0.940$. For use in model calculations the parameters recommended are as defined by the known oscillator strength. These are expected to provide estimated cross sections to 15% accuracy near threshold,

TABLE 1. Comparisons of Measured and Analytic Collision Strengths for the $Mg^+\ 3s\ ^2S \rightarrow 3p\ ^2P$ Transition

	Collision Strength $\Omega_{3s,3p}(E)$		
Energy E, eV	Analytic Best Fit	Analytic $f_{3s,3p} = 0.940$	Experiment
3.96	0.0	0.0	0.046
4.47	13.4	10.7	11.0
4.50	13.5	10.9	10.1
5.00	15.2	14.6	15.8
6.00	18.1	19.3	—
6.17	18.6	19.9	20.8
7.73	22.2	24.0	23.4
8.00	22.7	24.6	—
9.57	25.6	27.1	25.1
10.0	26.3	27.7	—
10.5	27.1	28.4	26.6
12.5	29.9	30.7	31.3
12.8	30.3	31.0	23.6
15.0	32.8	33.1	33.3
17.4	35.2	35.2	38.0
20.0	37.5	37.2	43.3
22.1	39.1	38.8	45.9
22.5	39.4	39.0	43.0
24.6	40.8	40.4	43.6
26.8	42.2	41.8	39.2
30.0	44.0	43.7	38.6
31.5	44.8	44.5	51.9
35.0	46.5	46.4	43.9
36.3	47.0	47.0	38.2
40.0	48.6	48.7	46.8

Statistical uncertainties in the last column at the 90% (1.7σ) confidence level are $^{+21}_{-18}$% (for $E \leq 8$ eV) and $^{+20}_{-16}$% (for $E > 8$ eV).

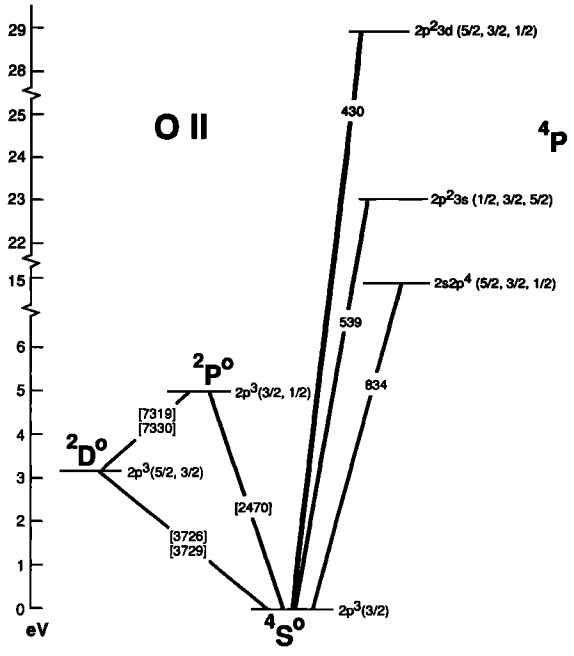

Fig. 3. Partial energy diagram of the levels of O II showing the lowest optically forbidden and optically allowed transitions.

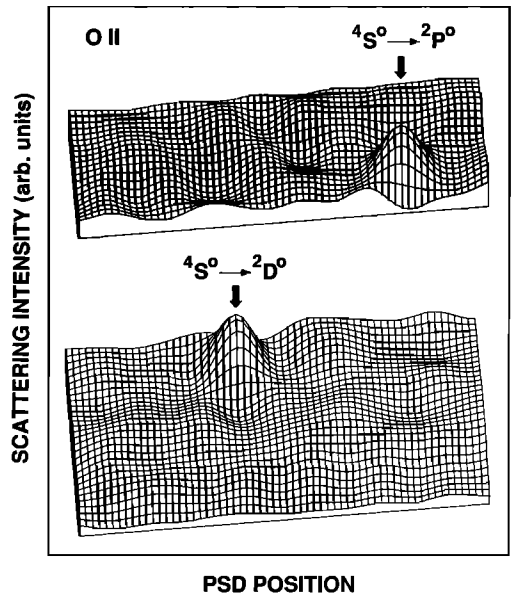

Fig. 5. Inelastic, energy-loss spectra of the O II optically forbidden $^4S^o \rightarrow 2s^22p^3\ ^2D^o$ transition (3726, 3729 Å or 3.33 eV) (bottom) and the $^4S^o \rightarrow 2s^22p^3\ ^2P^o$ transition (2470 Å or 5.02 eV) (top). The electron energies are 4.4 eV and 6.0 eV, respectively.

less accurate values near 40 eV, and increasingly accurate values above 100 eV. Table 1 gives values of the analytic cross section for selected energies, compared to the actual measured quantities.

The e-O II Scattering

Using the energy-loss, merged-beam approach, we have observed for the first time anywhere excitation of four transitions in O II. These are the first two optically allowed transitions ($^4S^o \rightarrow {}^4P$) and the first two optically forbidden transitions ($^4S^o \rightarrow {}^2D^o$ and $^2P^o$). A partial energy diagram of the relevant levels is shown in Figure 3. Measurements were taken within 2 eV of threshold for each excitation. The experimental "footprints" of the inelastic spectrum on the PSD for the optically allowed transitions are shown in Figure 4. The 833 Å line (Figure 4, bottom) is prominent both in the Io torus and in the Earth's dayglow emission. As summarized by *Shemansky* [1987], the collision strength Ω for excitation of the 833 Å multiplets is central to the determination of the O II density and oxygen/sulfur partitioning in the Io torus. Rate coefficients are obtained from collision strengths by integrating over a Maxwellian electron energy distribution. Footprints for the forbidden transitions in O II are shown in Figure 5. In the downward $^2D^o \rightarrow {}^4S^o$ transition the intensity ratio λ3729/λ3726 for the fine structure components is a frequently used diagnostic of electron density in gaseous nebulae [*Osterbrock*, 1989].

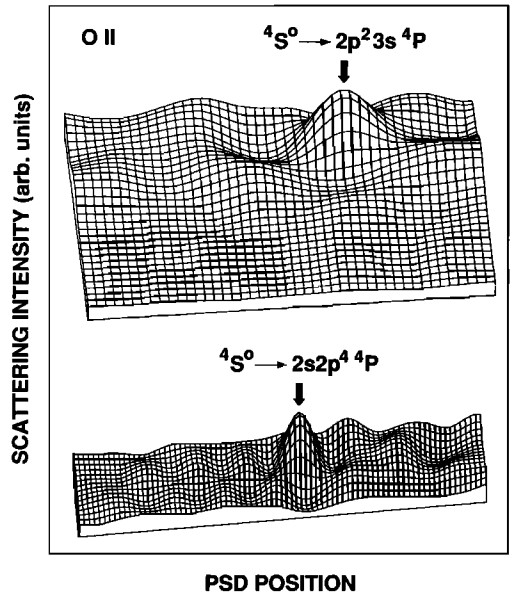

Fig. 4. Inelastic, energy-loss spectra of the O II optically allowed $2s^22p^3\ ^4S^o \rightarrow 2s2p^4\ ^4P$ transition (833 Å or 14.87 eV) (bottom) and the $2s^22p^3\ ^4S^o \rightarrow 2s^22p^23s\ ^4P$ transition (539.5 Å or 22.98 eV) (top). The electron energies are 17.8 eV and 24.5 eV, respectively.

It is likely that measurements of Ω for the optically forbidden transitions in O II (and also S II) will lead to further modifications of one's understanding of the Io torus O II and S II emission systems [*Shemansky*, 1987]. Observed intensities of the 833 Å transition from Voyager data have provided the basis of O II abundances in the torus. Accurate cross sections, especially in the threshold region (which emphasizes the electron energy distribution function), will increase the utility of this transition as a diagnostic of ion densities. While the 539 Å transiton is only weakly seen in the torus, its emissivity rapidly increases with electron temperature as more of the high-energy tail of the distribution function overlaps the threshold excitation cross section. And hence this transition can serve as a useful diagnostic of electron temperature. Work is currently in progress to measure accurate threshold excitation cross sections for these transitions, with due experimentalist's respect for the

fraction of metastable O II ions in the target beam! Results will be reported in a subsequent publication.

Acknowledgments. This work was carried out at the Jet Propulsion Laboratory, California Institute of Technology, and was supported by the National Aeronautics and Space Administration. Collaboration with the Queen's University (Belfast) was made possible through a NATO International Collaborative Research Grant. One of us (S.J.S.) acknowledges support from the NASA National Research Council for a Resident Research Associateship at JPL.

REFERENCES

Aggarwal, K. M., and A. Hibbert, Electron impact excitation with O III: Oscillator strengths and collision strengths, *J. Phys. B*, *24*, 3445, 1991.

Auerbach, D., R. Čačak, R. Caudano, T. D. Gaily, C. J. Keyser, J. W. McGowan, J. B. A. Mitchell, and S. F. J. Silk, Merged electron-ion beam experiments, I, Method and measurements of $(e-H_2^+)$ and $(e-H_3^+)$ dissociative-recombination cross sections, *J. Phys. B*, *10*, 3797, 1977.

Ballester, G. E., H. W. Moos, P. D. Feldman, D. F. Strobel, M. E. Summers, J.-L. Bertaux, T. E. Skinner, M. C. Festou, and J. H. Lieske, Detection of neutral oxygen and sulfur emissions near Io using IUE, *Astrophys. J.*, *319*, L33, 1987.

Bell, K. L., A. Hibbert, B. M. McLaughlin, and K. J. Higgins, Oscillator strengths for optically allowed transitions from the $2s^22p^3\ ^4S^o$, $^2D^o$ and $^2P^o$ states of singly ionized oxygen, *J. Phys. B*, *24*, 2665, 1991.

Blair, W. P., et al., Observations of a bright radiative filament in the Cygnus Loop with the Hopkins ultraviolet telescope, *Bull. Am. Astron. Soc.*, *23*, 917, 1991.

Broadfoot, A. L., B. R. Sandel, D. E. Shemansky, J. C. McConnell, G. R. Smith, J. B. Holberg, S. K. Atreya, T. M. Donahue, D. F. Strobel, and J.-L. Bertaux, Overview of the Voyager ultraviolet spectrometry results through Jupiter encounter, *J. Geophys. Res.*, *86*, 8259, 1981.

Brouillard, F., and W. Claeys, On the measurement of ion (atom)-ion(atom) charge exchange, in *Physics of Ion-Ion and Electron-Ion Collisions*, edited by F. Brouillard and J. W. McGowan, pp. 415–459, Plenum, New York, 1983.

Brown, R. A., A model of Jupiter's sulfur nebula, *Astrophys. J.*, *206*, L179, 1976.

Brown, R. A. Measurements of SII optical emission from the thermal plasma of Jupiter, *Astrophys. J.*, *224*, L97, 1978.

Burke, P. G., and D. L. Moores, Scattering of electrons by Mg^+ and Ca^+ ions, *J. Phys. B Proc. Phys. Soc., Ser. 2*, *1*, 575, 1968.

Carpenter, K. G., R. D. Robinson, G. M. Wahlgren, T. B. Ake, D. C. Ebbets, J. L. Linsky, A. Brown, and F. M. Walter, First results from the Goddard high-resolution spectrograph: The chromosphere of α Tauri, *Astrophys. J.*, *377*, L45, 1991.

Chutjian, A., and R. W. Newell, Experimental electron energy-loss spectra and cross sections for the $4^2S \rightarrow 4^2P$ transition in ZnII, *Phys. Rev. A*, *26*, 2271, 1982.

Ho, Y. K., and R. J. W. Henry, Oscillator strengths and collision strengths for OII and OIII, *Astrophys. J.*, *264*, 733, 1983*a*.

Ho, Y. K., and R. J. W. Henry, Oscillator strengths and collision strengths for SII, *Astrophys. J.*, *267*, 886, 1983*b*.

Ho, Y. K., and R. J. W. Henry, Oscillator strengths and collision strengths for SIII, *Astrophys. J.*, *282*, 816, 1984.

Kennedy, J. V., V. P. Myerscough, and M. R. C. McDowell, Electron impact excitation of the resonance lines of Be^+, Mg^+ and Ca^+, *J. Phys. B*, *11*, 1303, 1978.

Mewe, R., Interpolation formulae for the electron impact excitation of ions in the H-, He-, Li-, and Ne-sequences, *Astron. Astrophys.*, *20*, 215, 1972.

Mitroy, J., and D. W. Norcross, Electron-impact excitation of Al^{2+}, *Phys. Rev. A*, *39*, 537, 1989.

Mitroy, J., D. C. Griffin, D. W. Norcross, and M. S. Pindzola, Electron-impact excitation of the resonance transition in Ca^+, *Phys. Rev. A*, *38*, 3339, 1988.

Moos, H. W., et al., HUT spectra of the Io Torus, *Bull. Am. Astron. Soc.*, *23*, 940, 1991.

Osterbrock, D. E., *Astrophysics of Gaseous Nebulae and Active Galactic Nuclei*, p. 134, University Science Books, Mill Valley, Calif., 1989.

Shemansky, D. E., Ratio of oxygen to sulfur in the Io plasma torus, *J. Geophys. Res.*, *92*, 6141, 1987.

Shemansky, D. E., Energy branching in the Io plasma torus: The failure of neutral cloud theory, *J. Geophys. Res.*, *93*, 1773, 1988.

Shemansky, D. E., and G. R. Smith, The Voyager 1 EUV spectrum of the Io plasma torus, *J. Geophys. Res.*, *86*, 9179, 1981.

Shemansky, D. E., J. M. Ajello, D. T. Hall, and B. Franklin, Vacuum ultraviolet studies of electron impact excitation of helium: Excitation of He $n\ ^1P^o$ Rydberg series and ionization-excitation of He^+ nl Rydberg series, *Astrophys. J.*, *296*, 774, 1985*a*.

Shemansky, D. E., J. M. Ajello, and D. T. Hall, Electron impact excitation of H_2: Rydberg band systems and the benchmark dissociative cross section for H Lyman alpha, *Astrophys. J.*, *296*, 765, 1985*b*.

Smith, S. J., K.-F. Man, R. J. Mawhorter, I. D. Williams, and A. Chutjian, Absolute, cascade-free cross sections for the $^2S \rightarrow {}^2P$ transition in Zn^+ using electron energy-loss and merged-beams methods, *Phys. Rev. Lett.*, *67*, 30, 1991. (See also *American Institute of Physics Conference Proceedings, Ser. 233*, edited by J. Zorn and R. R. Lewis, pp. 363–365, American Institute of Physics, New York, 1991.)

Smith, S. J., A. Chutjian, J. Mitroy, S. S. Tayal, R. J. W. Henry, K.-F. Man, R. J. Mawhorter, and I. D. Williams, Excitation cross sections for the $ns\ ^2S \rightarrow np\ ^2P$ resonance transitions in Mg^+ ($n = 3$) and Zn^+ ($n = 4$) using electron energy-loss and merged-beams methods, *Phys. Rev. A*, in press, 1993.

Strobel, D. F., and J. Davis, Properties of the Io plasma torus inferred from Voyager EUV data, *Astrophys. J.*, *238*, L49, 1980.

Trauger, J. T., The Jovian nebula: A post-Voyager perspective, *Science*, *226*, 337, 1984.

van Regemorter, H., Rate of collisional excitation in stellar atmospheres, *Astrophys. J.*, *136*, 906, 1962.

Wåhlin, E. K., J. S. Thompson, G. H. Dunn, R. A. Phaneuf, D. C. Gregory, and A. C. H. Smith, Electron-impact excitation of Si^{3+} ($3s \rightarrow 3p$) using a merged-beam electron energy-loss technique, *Phys. Rev. Lett.*, *66*, 157, 1991.

Zapesochnyĭ, I. P., V. A. Kel'man, A. I. Imre, A. I. Daschenko, and F. F. Danch, Excitation of the Mg^+, Ca^+, Sr^+, and Ba^+ resonance levels in electron-ion collisions, *Sov. Phys. JETP, Engl. Transl.*, *42*, 989, 1976.

Zapesochnyĭ, I. P., A. I. Daschenko, V. I. Frontov, A. I. Imre, A. N. Gomonai, V. I. Lend'el, V. T. Navrotskii, and E. P. Sabad, Resonance structure of the cross section for electron-impact excitation of the $3p\ ^2P$ level of the magnesium ion, *JETP Lett.*, *39*, 51, 1984.

A. Chutjian and S. J. Smith, Jet Propulsion Laboratory, California Institute of Technology, Pasadena, CA 91109.

R. J. Mawhorter, Department of Physics and Astronomy, Pomona College, Claremont, CA 91711.

D. E. Shemansky, Department of Aerospace Engineering, University of Southern California, Los Angeles, CA 90089.

I. D. Williams, Department of Pure and Applied Physics, The Queen's University, Belfast BT7 1NN, United Kingdom.

(Received February 10, 1992;
revised October 29, 1992;
accepted November 29, 1992.)